THE ASIAN BULLETIN OF BIG DATA MANAGMENT
Vol. 6. Issue 1 (2026)
https://doi.org/10.62019/krfqm085

DFF-Net: Single Image Dehazing with Attention-based Deep Feature Fusion Network

Sanaullah Memon*, Adnan Baig, Hina Siddique Memon, Muhammad Awais Nawaz, Shagufta Aftab, Mashal Syed

Chronicle

Article history
Received: Feb 12, 2026
Received in the **revised format:** Feb 28, 2026
Accepted: March 15, 2026
Available online: March 30 2026

Sanaullah Memon* is currently affiliated with the Department of Information Technology, Shaheed Benazir Bhutto University Shaheed Benazirabad, Sindh Pakistan.
Email: sanaullah.memon_nf@sbbusba.edu.pk

Adnan Baig & Muhammad Awais Nawaz are currently affiliated with the Knowledge Unit of Systems and Technology, University of Management & Technology Lahore, Sialkot Campus.
Email: adnan.baig@skt.umt.edu.pk
Email: awais.nawaz@skt.umt.edu.pk

Hina Siddique Memon is currently affiliated with the Institute of Computer Science, Shah Abdul Latif University Khairpur, Sindh Pakistan.
Email: hinasanaullah52@gmail.com

Shagufta Aftab is currently affiliated with the Department of Computer Science, Ziauddin University Karachi, Sindh Pakistan
Email: shagufta.aftab@zu.edu.pk

Mashal Syed currently affiliated with the Department of Management Sciences, Alhamd Islamic University Quetta.
Email: mashal.syed@aiu.edu.pk

Corresponding Author*

Keywords: Convolution layer, Mixed convolution attention, Channel attention, Feature fusion, Feature extraction, Semantic loss.

© 2026 The Asian Academy of Business and social science research Ltd Pakistan.

Abstract

We suggest end-to-end convolution neural network for recovering a haze-free image from contaminated image. The feature extraction module enables network to extract the features at various levels. The network provides additional flexibility in dealing with different types of information and focuses more on important information using mixed convolution attention mechanism. To improve the dehazing performance, multi-level features are fused and further refined using feature fusion block. The good kernel estimation can recover a sharp image. Moreover, DFF-Net has ability to capture sharp textural and semantic information, and recover high-quality haze-free image. Furthermore, semantic differences in deep features are measured by deep semantic loss. The experimental findings demonstrate that our suggested method exhibits superior performance compared to other haze-removal methods on both synthetic and real-world images.

INTRODUCTION

Haze is an unanticipated environmental consequence induced by the absorption of light and tiny particles in the atmosphere, which affects the quality of image [1]. The quality of image degrades dramatically due to poor clarity, low contrast, color distortion, and blurring. Image dehazing has gained consideration in the field of computer vision during last twenty years. Numerous methods have been developed to restore a dehazed image from a degraded one. Image degradation is often modeled using an atmospheric scattering model [2].

$$I_h(p) = J(p)T_m(p) + A(p)(1 - T_m(p)) \quad (1)$$

Where I_h denotes the actual hazy image, p denotes the pixel position, J denotes the scene radiant image, A denotes the global atmospheric light, and T_m denotes the transmission map. Image dehazing is a complicated issue owing to unidentified transmission map and atmospheric light for each pixel. To tackle this issue, He *et al.* [3] suggested the dark channel prior to approximate the unidentified parameters, using a soft matting interpolation method and haze imaging model. Tan *et al.* [4] proposed a high local contrast method, which could not accurately portray the features of real-world images. In contrast to the conventional methods, the methods based on deep learning are accomplished exceptional advancements in image segmentation, classification, and fusion [5-10]. The impressive dehazing performance is shown by these methods. In this paper, the attention-based deep feature fusion network (DFF-Net) is developed for recovering haze-free image in view of the following aspects.
The recovery of dehazed image is essential for image dehazing. It is difficult to preserve shallow feature information at deep neural network. The haze degrades many non-haze details which reduces the visual quality of final dehazed image. Moreover, many convolution neural networks will not be able to cover all channels and pixels when different channel features are treated equally. To solve this problem, an appropriate method is needed for recovering dehazed image with significant details to better visualize the pleasing results.
The three key contributions of this study are stated below:

- We have developed end-to-end attention-based deep learning method named deep feature fusion network (DFF-Net). The mixed convolution attention is integrated with channel attention which enables network to focus more on the important features at various resolution levels.
- DFF-Net has ability to fuse and further refine feature maps in full connection manner using feature fusion method. The feature fusion block accepts all feature maps of various levels and improves internal features representation. These feature maps contain both the image details and semantic information which are in favor of restoration of clear image.
- Deep semantic loss is employed for measuring the semantic differences between ground truth image and haze-removed outcomes obtained from deep features.

RELATED WORK

Initially, image dehazing required a large number of images depicting the same scene under various conditions. It is more difficult to remove haze from images when there is no additional information available [11]. Several methods are suggested for image dehazing, relying on the development of physical scattering model Eq. (1) [12]. These methods fall under the categories of prior-based image dehazing methods, and deep learning-based image dehazing methods.

PRIOR-BASED IMAGE DEHAZING METHODS

Prior-based methods of image dehazing utilize image properties to analyze unidentified parameters of atmospheric scattering model. He *et al.* [3] suggested the dark channel prior to analyze images and transmission maps influenced by haze. The underlying assumption in the regions lacking haze will exhibit reduced intensity levels in one or more color channel. This method was efficient for images with relatively dark haze and entailed significant computational power. An efficient regularization algorithm for recovering dehazed images was suggested by Meng *et al.* [13]. This method analyzed the underlying edge constraints. Berman *et al.* [14] developed a

prior-based method which asserted that the pixels are non-local in a particular cluster and each cluster in the haze-free image can be represented by a line in RGB space. The haze lines proved useful in reconstructing the haze-free image. The color attenuation prior method was developed by Zhu *et al.* [15]. It involved calculating the transmittance, restoring the radiance of scene through a linear model, and creating a link between the spatial information of the hazy image and its properties.

Deep learning-based image dehazing methods

The problem of single image dehazing has been addressed using deep learning algorithms in recent times. Ren *et al.* [16] suggested deep neural network. It removed haze from a single image at different scales. The network assigned weights between hazy image and its transmission map. The coarse-scale net was liable for computing transmission map based on entire image, while the fine-scale network further improved it. Cai *et al*. [17] suggested DehazeNet. It approximated the transmission medium to reconstruct a dehazed image. This network took the hazy image and its transmission map using atmospheric scattering model. However, a significant drawback with the above approaches is the dependence on precise atmospheric light and transmission map for the better quality reconstruction output. In case, where predicted transmission map is erroneous, guided image filtering is necessary to filter the transmission map [18]. Li *et al.* [19] proposed AOD-Net, which produced a haze-free image directly using CNN. This approach employed a variable K to merge the atmospheric light and transmission map into a single equation. Consequently, AOD-Net was limited by the inadequacy of its physical model. Ren *et al.* [20] proposed a gated fusion network that generated haze-free image by extracting relevant features from three derived inputs. However, the complete network is intricate and requires a significant amount of time to execute. Furthermore, the model is not capable of processing images that have an excessive amount of haze and distortion. Chen *et al.* [21] introduced GCA-Net, which leveraged enhanced dilated convolution and a gated fusion sub-network to differentiate between a foggy and clear image. This approach reduced gridding artifacts and could not be suitable for generating extremely accurate information. In contrast, Xiao *et al*. [22] introduced GMAN. This approach utilized bottleneck residual blocks in network for producing excellent results using commonly available dehazing datasets. Liu *et al.* [23] developed GridDehazeNet. It utilized attention-based multi-scale evaluation for removing haze. This approach improved haze reduction and distortion control. Qin *et al.* [24] proposed an attention network which enhanced the visual quality and color fidelity of images by fusing features and employing local and global residual learning. S. Memon *et al.* [25] presented AMSFF-Net that employed an encoder-decoder structure of network for reducing artifacts and producing brightness variance with less color distortion.

Deep Feature Fusion Network (DFF-Net)

The DFF-Net is shown in Fig. 1. Firstly, a hazy image is processed by shallow feature extraction part for feature extraction and then fed into three group structures with skip connections. In each group structure, the features are focused using the feature extraction module, channel attention and mixed convolution attention block. It obtains features at various levels and deals with different types of information allowing network to concentrate on important features. The fusion method is performed among features of different resolution levels using feature fusion block. Then, fused features are forwarded to reconstruction part to recover the haze-free images.

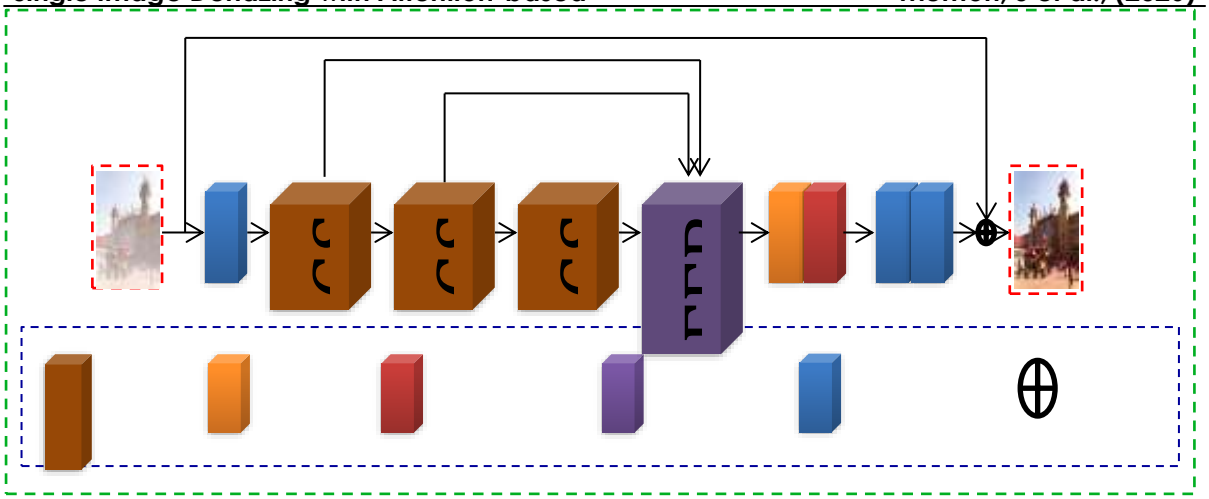

Figure1.
The structure of deep feature fusion network (DFF-Net)

Group Structure (GS)

The three-group structure includes the feature extraction module, channel attention, mixed convolution attention, local and global residual learning, and skip connections. It improves the efficacy of the network. The local residual learning enables the network to bypass less significant information through numerous local residual connections while the network concentrates on the useful information. Finally, the haze-free image is recovered using the global residual learning module. Fig.2 depicts the group structure (GS).

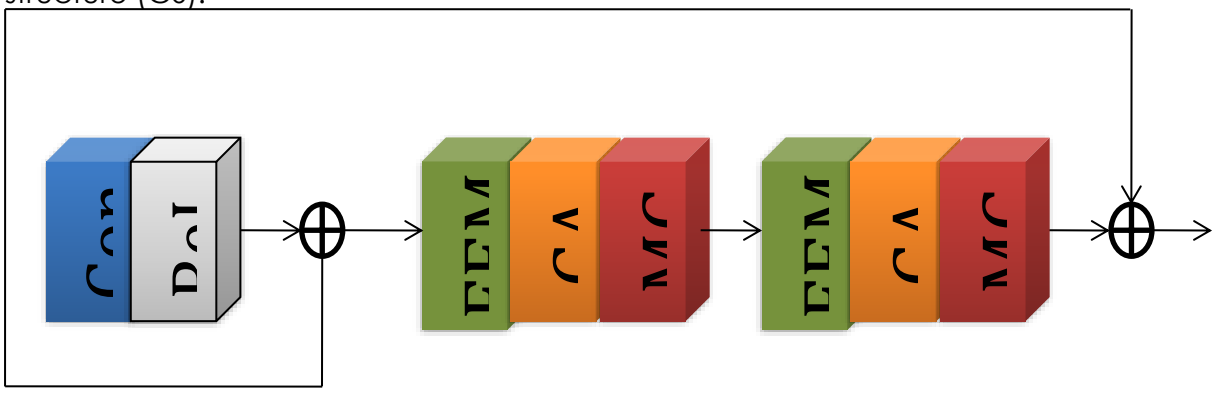

Figure 2.
Group structure (GS)

Feature Extraction Module (FEM)

Typically, using features extracted from individual layer are insufficient. The features from initial layers primarily emphasize basic details like edge and shape, which is important for object positioning and image structure recovery. Meanwhile, the features from later layers contain more meaningful semantic information, which assists in retaining textural and color information effectively. Fig. 3 depicts the structure of feature extraction module, which includes convolution layers and ReLU activation functions. The first layer employs a 3x3 convolution with a stride of 2. This reduces the resolution of feature map by half and double the width. While the sequence of 3x3 convolution layer, ReLU, and 3x3 convolution layer is employed to compute the output features respectively.

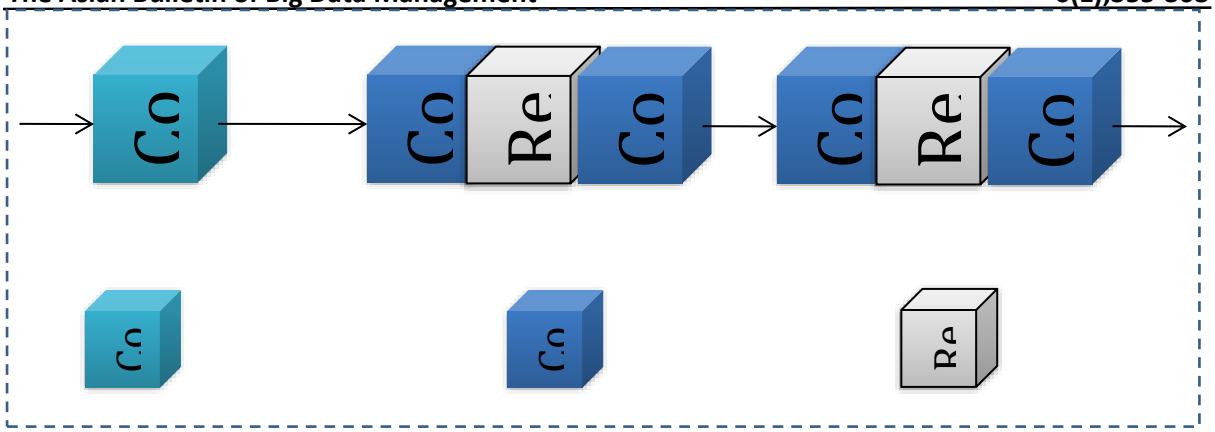

Figure 3.
The structure of the feature extraction module

Channel Attention (CA)

The channel attention mechanism concentrates on various features of the image and boosts the different channels for different features. The formation of channel attention is illustrated in Fig. 4. The shape of feature maps transforms from *CxHxW* to *Cx1x1*, where *C, H,* and *W* represents the channel, height, and width. The feature maps are then passed through two convolution layers, ReLU, and sigmoid activation function to achieve different channel weights. The element-wise product combines the channel attention map with the input feature map F_i to construct the output feature map needed for mixed convolution attention mechanism. Eq. (2) represents the channel attention mechanism.

$$F_c = F_i \otimes (\sigma(Conv(\delta(Conv(AvgPool(F_i)))))) \quad (2)$$

Here, *AvgPool(.)* represents the average pooling layer, *Conv* represents the convolution layer, δ represents the ReLU layer, σ represents the sigmoid function, F_i represents the input to the channel attention, $\otimes$ represents the element-wise product, and F_c represents the channel attention output.

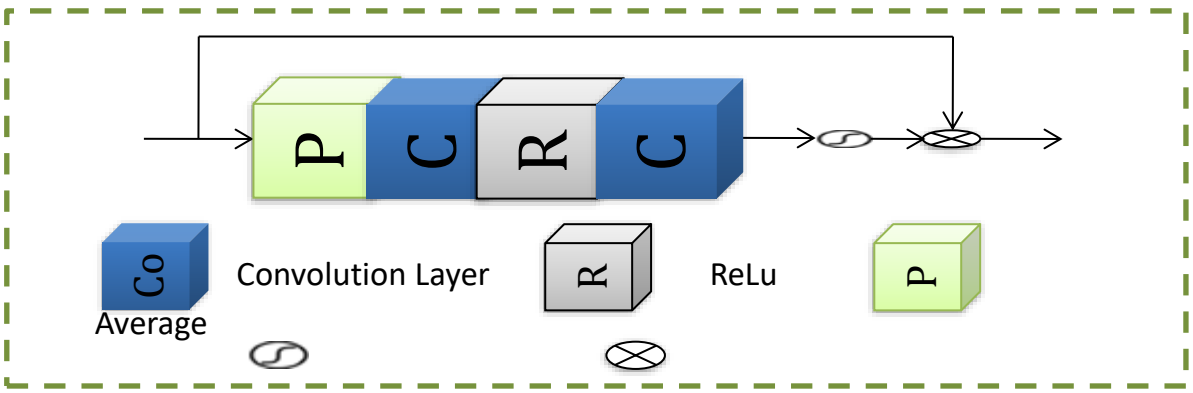

Figure 4.
The formation of channel attention

Mixed Convolution Attention (MCA)

The distribution of haze is irregular among distinct pixels in an image. The mixed convolution attention block is utilized to put more emphasis on important features. Moreover, many haze-removal attention methods ignore the kernel size used in distinct convolution layers. For each channel, employing kernel sizes individually and ignoring their impact within a single layer is the concept behind depthwise convolution [26]. The shape of mixed depth-wise convolution layer (MDCL) is illustrated in Fig. 5. The results of the channel attention mechanism are analyzed here

using mixed convolution attention block that comprises of mixed depthwise convolution layer, ReLU activation function, pointwise convolution layer, and sigmoid activation function as shown in Fig. 6. The kernel size of *1x1* for the pointwise convolution layer is employed efficiently to use the information of input features in the same spatial region. This generates a feature map with reduced number of channels from *C* to *1*. Consequently, each pixel in the region receives different attention from network. Eq. (3) represents the mixed convolution attention mechanism.

$$F_m = F_c \otimes (\sigma(Conv_p(\delta(Conv_m(F_c))))) \quad (3)$$

Here, $Conv_m$ represents mixed depthwise convolution layer, δ represents ReLU activation function, $Conv_p$ represents pointwise convolution layer, σ represents sigmoid activation function, $\otimes$ represents element-wise product, F_c represents the output of channel attention, and F_m represents the output of mixed convolution attention.

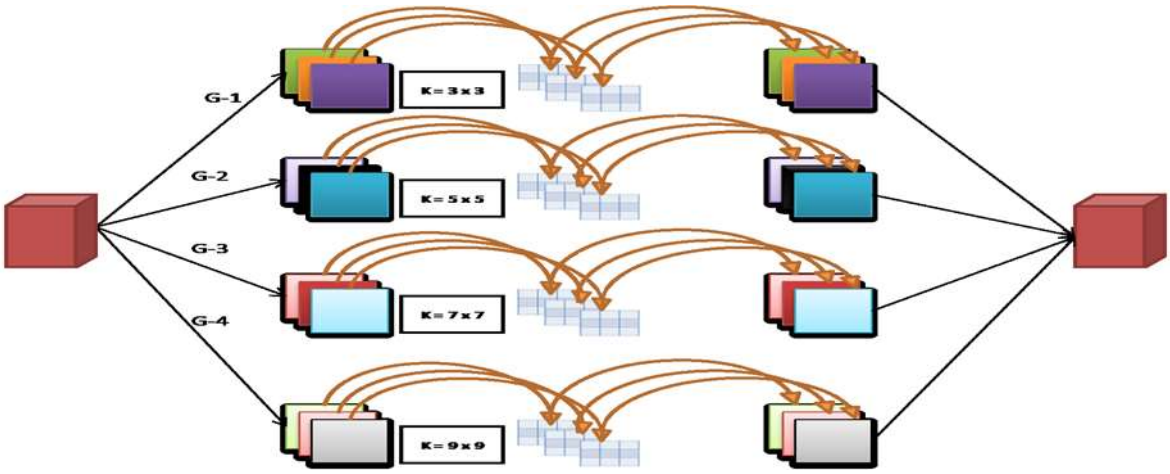

Figure 5.
The shape of MDCL

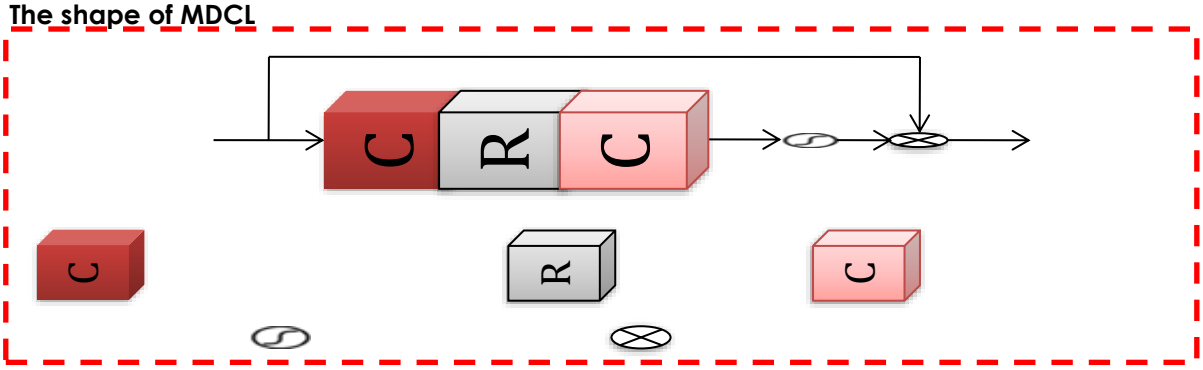

Figure 6.
The formation of mixed convolution attention block

Feature Fusion

The feature maps produced at various levels donot have equal importance. The feature fusion method is employed to fuse feature maps using feature fusion block (FFB). The three steps such as rescaling, integrating and refining play crucial role in feature fusion process. The inputs Z_1, Z_2, and Z_3 represent the feature maps at three levels and rescaled them to intermediate resolution that is the resolution of Z_2. Let b_1, b_2, and b_3 show the relative significance of the feature maps of three levels. The integrated features Z_n are expressed in Eq. (4). Since the feature maps contain both the image details and semantic information of an image, which clearly supports the enhancement of images without haze. However, to improve the feature representation for the dehazing purpose, the feature maps are further refined

applying 3x3 convolution layer on the fused features, resulting in the refined features maps.

$$Z_n = \sum_{j=1}^{3} b_j Z_j \quad (4)$$

Loss Function

The three loss functions are utilized to calculate statistical difference between recovered images and their equivalent ground truth images. These loss functions are explained below.

Smooth L1

By default, we use smooth L1 loss which is less receptive to outliers than L2 loss and maintain accuracy at low frequencies. It helps to prevent the problem of gradient explosion. Eq. (5) and Eq. (6) provide a description of the loss function.

$$L_{smo} = \frac{1}{CHW}\psi(I' - I), \quad (5)$$

$$\psi(e) = \begin{cases} 0.5e^2, & if\ |e| < 1, \\ |e| - 0.5, & otherwise. \end{cases} \quad (6)$$

The recovered image is represented by *I'*, and the equivalent ground truth image is represented by *I*. Channel is represented by *C*, height is represented by *H*, and width is represented by *W*, respectively. Additionally, if the absolute error |e| is less than 1, the gradient value will be 1.

Perceptual Loss

Perceptual loss is employed to compute the variance between the recovered image *I'* and the ground truth image *I*. The pre-trained deep learning network, specifically VGG16 is employed for feature extraction from the final layers. The perceptual loss function is described below in Eq. (7).

$$L_{per} = \sum_{j=1}^{N} \frac{1}{C_j H_j W_j} \left\| \emptyset_j(I') - \emptyset_j(I) \right\|_2^2, \quad (7)$$

The ground truth image *I* and the recovered image *I'* are correlated to theVGG16 feature maps and denoted by $\emptyset(I)$ and $\emptyset(I')$, respectively. The dimensions of $\emptyset(I)$ and $\emptyset(I')$ are described by C_j, H_j, and W_j, where $j = 1, 2, \ldots N$.

Deep Semantic Loss

In deep features, the spatial correlation and the boundary details are emphasized by deep semantic loss. The interpretation of Laplace operator [27] demonstrates semantic details present in observed features with significant variations. A description of the deep semantic loss is provided in Eq. (8).

$$L_{sem} = \sum_{j=1}^{N} \frac{j}{C_j H_j W_j} \left\| \delta_1 \left(\xi \left(\emptyset_j(I') \right) \right) - \delta_1 \left(\xi \left(\emptyset_j(I) \right) \right) \right\|_1, \quad (8)$$

The ReLU function is represented by δ, and the Laplace operator is shown by $\xi(.)$.The aspects of feature maps such as $\emptyset(I')$ and $\emptyset(I)$ are described by C_j, H_j, and W_j, where $j = 1, 2 \ldots N$. To achieve deep semantic information, the recovered image *I'* has been compared to the ground truth image *I* using the L1 norm.

Total Loss

The deep semantic loss, perceptual loss, and smooth L1 loss comprise the total loss. Eq. (9) illustrates that the loss function reduces throughout the training process to refine the model.

$$L_{total} = L_{smo} + \lambda_1 L_{per} + \lambda_2 L_{sem}, \quad (9)$$

The interaction of the loss components is controlled by λ_1 and λ_2.

Experiments

Various experiments are accomplished to assess the efficiency of suggested method by comparing it with the other haze-removal methods using both the SOTS and real-world images.

Implementation Details

The suggested network consists of feature extraction modules, channel attention, mixed convolution attention, and feature fusion block. The convolution layers possess kernel size of *3×3* except for channel attention which has convolution layer with a kernel size of *1×1*. The mixed convolution attention block consists of mixed depthwise convolution layer, ReLU, and pointwise convolution layer with a kernel size of *1×1*. The size of all feature maps is fixed, and the output of each level is 64 filters.

Training Settings

The pytorch is employed to implement the suggested network with a 240x240 input size. The Adam optimizer [28] is used for swift training, and the values are adjusted to 0.9 and 0.999 for β_1 and β_2. The initial value for learning rate is 0.0001.We used the GeForce GTX 1080Ti GPU to instruct the network for 100 epochs on ITS and 50 epochs on OTS.

Datasets and Evaluation Indexes

The suggested network is trained and tested using RESIDE dataset [29]. For indoor training set (ITS), A∈[0.7, 1.0] and β∈[0.6, 0.8] were utilized to create 13990 indoor hazy images from 1399 indoor clear images. Middlebury Stereo [30] and NYU Depth V2 [31] datasets were utilized to generate depth maps. For outdoor training set (OTS), A∈[0.8, 1.0] and β∈[0.04, 0.2] were utilized to create 296695 outdoor hazy images from 8477 outdoor clear images. The depth maps of outdoor images were created using the algorithm suggested in [32]. The SOTS dataset is employed for testing purpose. It includes 500 indoor and 500 outdoor hazy images. We evaluate the performance of various methods of image dehazing using PSNR and SSIM.

Performance Analysis on Synthetic Dataset

Experimental evaluations on the synthetic dataset are executed to assess the performance of suggested method and numerous other methods. Fig. 7 and Fig. 8 demonstrate qualitative results on synthetic indoor and outdoor images. The images produced by DCP method [3] are darker than comparable ground truth images. This method frequently exhibits severe distortion of color and loss of depth information, indicating that the prior-based approach is ineffective at solving the problem (see Figs. 7(b) and 8(b)). AOD-Net [19] exhibits better performance in color restoration when compared to DCP. It still leaves a hazy effect and halo artifacts in the corners and edges (see Figs. 7(c) and 8(c)). GCA-Net [21] achieves impressive dehazing performance by reducing gridding artifacts and improving the edges and texture details (see Figs. 7(d) and 8(d)). GridDehazeNet [23] removes color distortion and generates haze-free images. The haze-free images are more similar to ground truth images, but it leaves certain artifacts in its wake while removing dense haze (see Figs. 7(e) and 8(e)). AMSFF-Net [25] works better to lessen haze, brightness variation, and color distortion while producing fewer artifacts in an image (see Figs. 7(f) and 8(f)).

FFA-Net [24] accomplishes excellent dehazing outcomes by avoiding excessively sharp edges and color erosion (see Figs. 7(g) and 8(g)). It restores color in most areas of images. However, it cannot remove haze from the images successfully. Our suggested method generates the best haze-free image, reduces color distortion, and restores images with sharp textural and semantic details (see Figs. 7(h) and 8(h)). Table 1 and Table 2 present quantitative outcomes of several dehazing methods on synthetic indoor and outdoor images. Deep learning-based dehazing methods exhibit better values of PSNR and SSIM than prior-based methods. Additionally, our suggested method recovers dehazed images with maximum PSNR and SSIM values compared to all other currently used dehazing methods on SOTS.

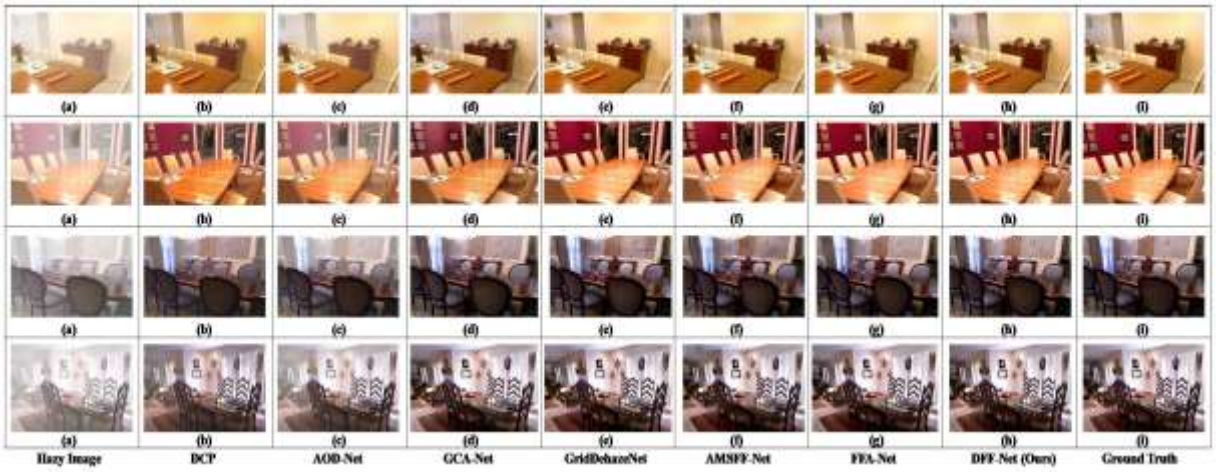

Figure 7.
Qualitative results on indoor images of SOTS with various dehazing methods

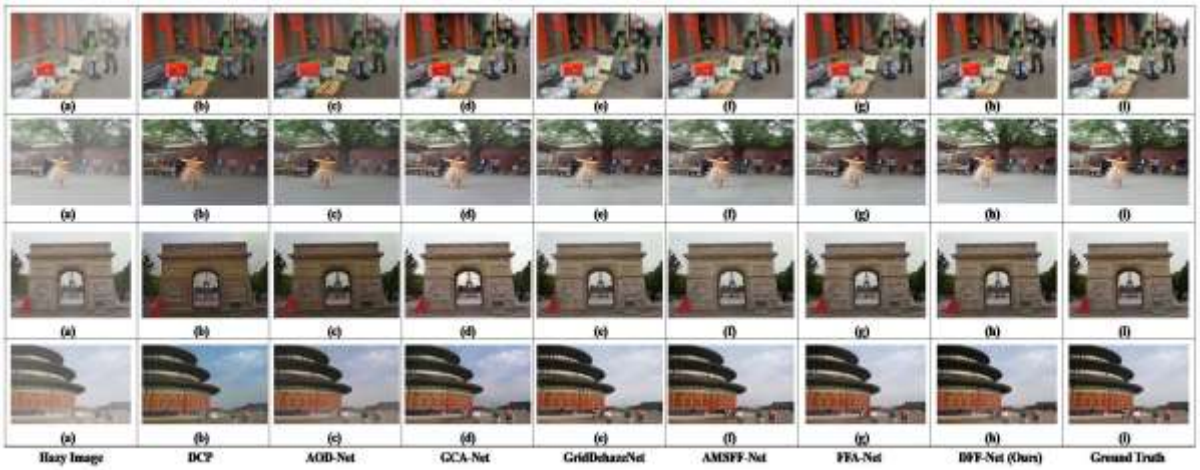

Figure 8.
Qualitative results on outdoor images of SOTS with various dehazing methods

Performance Analysis on Real-World Dataset

We evaluate the suggested method with numerous other dehazing methods using unannotated hazy images of the ExternelCvpr dataset. The haze-free images of dataset are not available. We have only measured the qualitative results of real-world images as shown in Fig. 9. The observations are generally reliable with those on the synthetic images. The outcomes of DCP [3] exhibit the darker images with severe color distortions (see Figs. 9(b)). The haze cannot be completely removed by AOD-Net [19]. It reveals the brightness degradation and generates halo effects around edges of object (see Figs. 9(c)). The outcomes of GCA-Net [21] exhibit the missing regions and

brightness variance. It also reduces gridding artifacts in images (see Figs. 9(d)). The AMSFF-Net [25] generates fewer artifacts in image. This network is more efficient in reducing haze, brightness variance, and color distortions (see Figs. 9(e)). The FFA-Net [24] removes thin haze effectively. Moreover, it generates some apparent tiny artifacts in specific regions and eliminates color distortion (see Figs. 9(f)). In comparison with aforementioned methods, our suggested method is more effective in reducing haze and managing distortions. It offers an immense cooperation between restoration of color fidelity and severity of dehazing (see Figs. 9(g)).

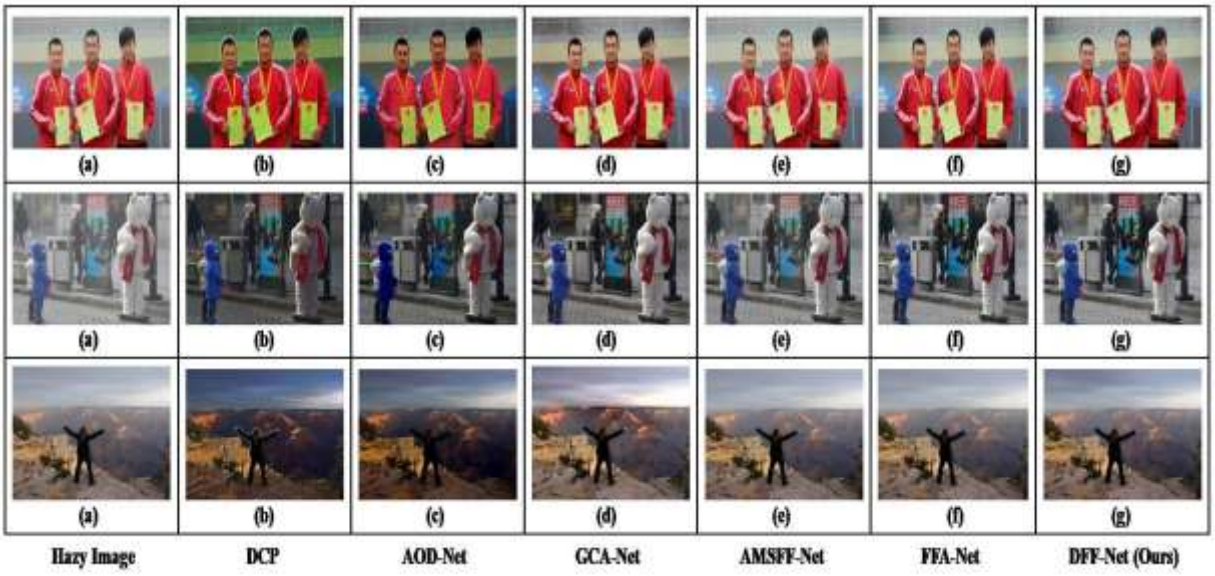

Figure 9.
Qualitative results on unannotated real-world images with various dehazing methods

Table 1.
Quantitative outcomes of several dehazed methods on indoor images of SOTS dataset

Methods	DCP [3]	AOD-Net [19]	GCA-Net [21]	GridDehazeNet [23]	AMSFF-Net [25]	FFA-Net [24]	DFF-Net (Ours)
PSNR	16.16	20.51	21.69	32.16	34.87	36.39	**37.42**
SSIM	0.8546	0.8162	0.8621	0.9836	0.9899	0.9886	**0.9925**

Table 2.
Quantitative outcomes of several dehazed methods on outdoor images of SOTS dataset

Methods	**DCP [3]**	**AOD-Net [19]**	**GCA-Net [21]**	**GridDehazeNet [23]**	**AMSFF-Net [25]**	**FFA-Net [24]**	**DFF-Net (Ours)**
PSNR	19.14	24.14	22.96	30.86	32.23	33.57	**34.64**
SSIM	0.8605	0.9198	0.8911	0.9819	0.9854	0.9840	**0.9889**

The suggested method outperforms existing haze removal methods in terms of PSNR and SSIM values on indoor and outdoor images, demonstrating its relevance in retrieving haze-free images without affecting image quality and preserving glamorous images with sharp textural details. We evaluated efficiency of deep semantic loss through a number of tests and selected the best average assessment outcomes after one hundred iterations on training of model, as illustrated in Fig. 10. The model performance and dehazing efficiency is improved by deep semantic loss.

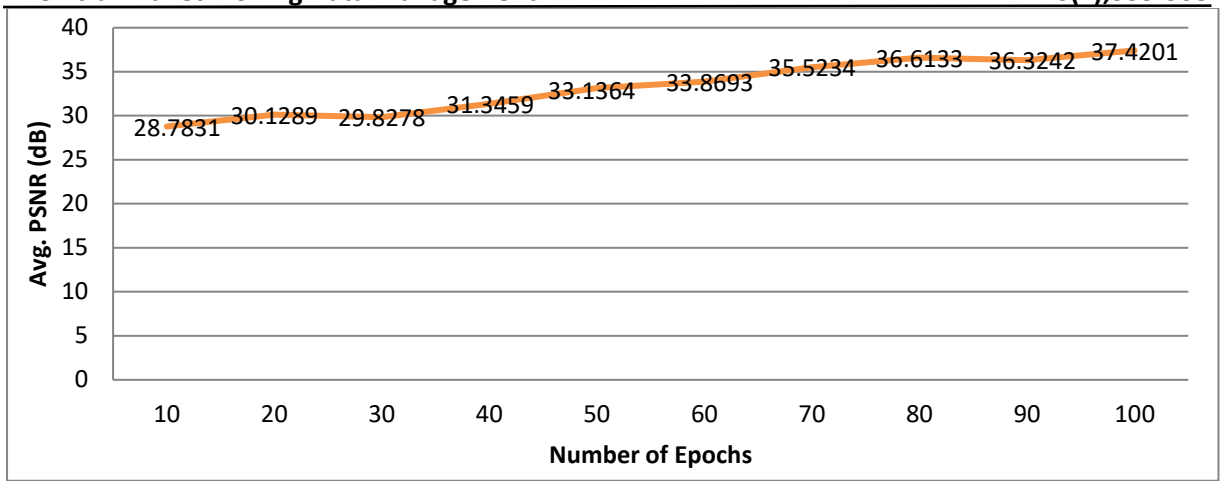

Figure 10.
Average assessment outcomes on training with the indoor images

Runtime Analysis

We analyzed the running time of aforementioned state-of-the-art methods on SOTS to assess efficiency and depicted their average runtimes in Fig. 11. Using our proposed method, one image from SOTS is dehazed in an average time of 14.6 milliseconds. The proposed method comes in the second place among the evaluated dehazing methods. The running time is less than all other dehazing methods except AOD-Net [19]. AMSFF-Net [25] and GridDehazeNet [23] take approximately 2 ms and 4 ms more than our proposed method.

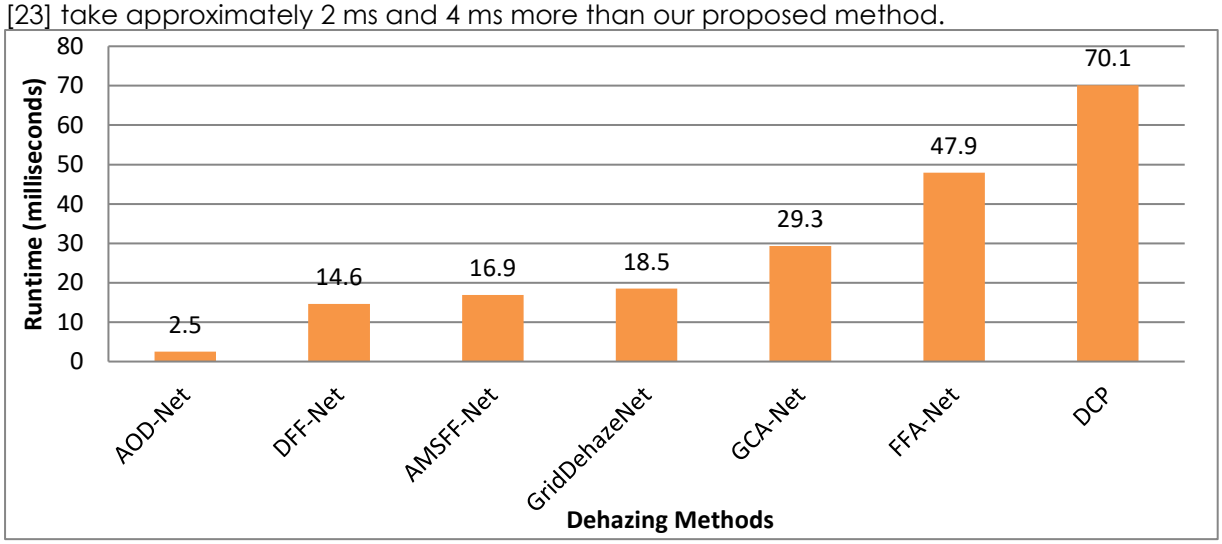

Figure 11.
Average runtime of evaluated dehazing methods on SOTS

Ablation Analysis

We conduct an ablation analysis to demonstrate the efficiency of our proposed network. The analysis considers different components and loss function, including feature extraction module, channel attention, mixed convolution attention, and deep semantic loss. We utilize the similar configuration to instruct the network as described in the implementation details (section 4.1). The outcomes of the fusion of several components are displayed in Table 3. The image dehazing task involves the evaluation of four different network architectures. Base network is developed using feature extraction modules and feature fusion and maintaining the loss strategy. The performance of network with feature extraction modules is consistently satisfactory in extracting feature information and image details. The network is developed integrating the channel attention with feature extraction modules. It removes haze and handles areas with more details but still donot accentuate semantic and textural details. Besides, the channel attention and mixed convolution attention mechanism is utilized to

develop network without deep semantic loss. It focuses on the important features and enhances performance by capturing the semantic and textural details from extracted features. When the network is trained with deep semantic loss, it improves the model performance and dehazing efficiency. The ablation findings demonstrate that each component has a considerable impact on the performance of network. It helps in restoring the textural details and reducing the color distortion to enhance the effectiveness of the image dehazing network.

Table 3.
Comparison on SOTS indoor testset using several components

Feature extraction module	✓	✓	✓	✓
Channel attention	---	✓	✓	✓
Mixed convolution attention	---	---	✓	✓
Deep semantic loss	---	---	---	✓
PSNR	32.85	34.62	36.89	37.42
SSIM	0.9698	0.9769	0.9892	0.9925

LIMITATIONS

When the image boundary is unclear, the proposed method generates images with distorted low-frequency color areas. This indicates that the method lacks the necessary robustness to function effectively in complex situations.

CONCLUSION

An end-to-end attention-based deep feature fusion network is proposed to recover haze-free image. The network has ability to extract features from shallow to deep layers using feature extraction modules. Channel features are focused by channel attention mechanism. Mixed convolution attention block pays more attention to important features. It transforms redundant features into useful ones and produces clear image with the sharp textural and semantic details. The deep semantic loss enables network to measure semantic differences between ground truth images and haze-removed outcomes. The experimental findings illustrate that DFF-Net improves the dehazing performance on both the synthetic and real-world images compared with other haze-removal methods. It improves the quality of haze-free image and reduces color distortion.

DECLARATIONS

Acknowledgement: We appreciate the generous support from all the contributors to the research and their different affiliations.
Funding: No funding body in the public, private, or nonprofit sectors provided a particular grant for this research.
Availability of data and material: In the approach, the data sources for the variables are stated.
Authors' contributions: Each author participated equally in the creation of this work.
Conflicts of Interest: The authors declare no conflict of interest.
Consent to Participate: Yes
Consent for publication and Ethical approval: Because this study does not include human or animal data, ethical approval is not required for publication. All authors have given their consent.

References

H. Rashid, N. Zafar, M. J. Iqbal, H. Dawood, and H. Dawood, "Single Image Dehazing using CNN," *Procedia Comput. Sci.*, vol. 147, pp. 124–130, 2019, doi: 10.1016/j.procs.2019.01.201.

H. Zhang and V. M. Patel, "Densely Connected Pyramid Dehazing Network," *Proc. IEEE Comput. Soc. Conf. Comput. Vis. Pattern Recognit.*, pp. 3194–3203, 2018, doi: 10.1109/CVPR.2018.00337.

K. He, J. Sun, and X. Tang, "Single image haze removal using dark channel prior," *IEEE Trans. Pattern Anal. Mach. Intell.*, vol. 33, no. 12, pp. 2341–2353, 2011, doi: 10.1109/TPAMI.2010.168.

R. T. Tan, "Visibility in bad weather from a single image," *26th IEEE Conf. Comput. Vis. Pattern Recognition, CVPR*, 2008, doi: 10.1109/CVPR.2008.4587643.

K. Simonyan and A. Zisserman, "Very deep convolutional networks for large-scale image recognition," *3rd Int. Conf. Learn. Represent. ICLR 2015 - Conf. Track Proc.*, pp. 1–14, 2015.

W. Weng and X. Zhu, "INet: Convolutional Networks for Biomedical Image Segmentation," *IEEE Access*, vol. 9, pp. 16591–16603, 2021, doi: 10.1109/ACCESS.2021.3053408.

A. Handa, P. Garg, and V. Khare, "Masked Neural Style Transfer using Convolutional Neural Networks," *2018 Int. Conf. Recent Innov. Electr. Electron. Commun. Eng. ICRIEECE 2018*, pp. 2099–2104, 2018, doi: 10.1109/ICRIEECE44171.2018.9008937.

J. Pang, K. Chen, J. Shi, H. Feng, W. Ouyang, and D. Lin, "Libra R-CNN: Towards balanced learning for object detection," *Proc. IEEE Comput. Soc. Conf. Comput. Vis. Pattern Recognit.*, vol. 2019-June, no. 3, pp. 821–830, 2019, doi: 10.1109/CVPR.2019.00091.

W. Ren *et al.*, "Gated Fusion Network for Single Image Dehazing," *Proc. IEEE Comput. Soc. Conf. Comput. Vis. Pattern Recognit.*, pp. 3253–3261, 2018, doi: 10.1109/CVPR.2018.00343.

S. Woo, J. Park, J. Y. Lee, and I. S. Kweon, "CBAM: Convolutional block attention module," *Lect. Notes Comput. Sci. (including Subser. Lect. Notes Artif. Intell. Lect. Notes Bioinformatics)*, vol. 11211 LNCS, pp. 3–19, 2018, doi: 10.1007/978-3-030-01234-2_1.

S. K. Nayar and S. G. Narasimhan, "Vision in bad weather," *Proc. IEEE Int. Conf. Comput. Vis.*, vol. 2, pp. 820–827, 1999, doi: 10.1109/iccv.1999.790306.

G. Fan, Z. Hua, and J. Li, "Multi-scale depth information fusion network for image dehazing," *Appl. Intell.*, vol. 51, no. 10, pp. 7262–7280, 2021, doi: 10.1007/s10489-021-02236-2.

G. Meng, Y. Wang, J. Duan, S. Xiang, and C. Pan, "Efficient image dehazing with boundary constraint and contextual regularization," *Proc. IEEE Int. Conf. Comput. Vis.*, pp. 617–624, 2013, doi: 10.1109/ICCV.2013.82.

D. Berman, "Non-Local Image Dehazing," *Proc. IEEE Conf. Comput. Vis. Pattern Recognit.*, pp. 1674–1682, 2016.

Q. Zhu, J. Mai, and L. Shao, "A Fast Single Image Haze Removal Algorithm Using Color Attenuation Prior," *IEEE Trans. Image Process.*, vol. 24, no. 11, pp. 3522–3533, 2015, doi: 10.1109/TIP.2015.2446191.

W. Ren, J. Pan, H. Zhang, X. Cao, and M. H. Yang, "Single Image Dehazing via Multi-scale Convolutional Neural Networks with Holistic Edges," *Int. J. Comput. Vis.*, vol. 128, no. 1, pp. 240–259, 2020, doi: 10.1007/s11263-019-01235-8.

B. Cai, X. Xu, K. Jia, and C. Qing, "DehazeNet : An End-to-End System for Single," *Ieee Trans. Image Process.*, vol. 25, no. 11, pp. 5187–5198, 2016.

K. He, J. Sun and X. Tang, "Guided Image Filtering," in *IEEE Transactions on Pattern Analysis and Machine Intelligence*, vol. 35, no. 6, pp. 1397-1409, June 2013, doi: 10.1109/TPAMI.2012.213.

B. Li, X. Peng, Z. Wang, J. Xu, and D. Feng, "(AOD-Net) - AOD-Net:All-in-One Dehazing Network Boyi," *Proc. IEEE Int. Conf. Comput. Vis.*, pp. 4770–4778, 2017.

W. Ren *et al.*, "Gated Fusion Network for Single Image Dehazing," *Proc. IEEE Comput. Soc. Conf. Comput. Vis. Pattern Recognit.*, pp. 3253–3261, 2018, doi: 10.1109/CVPR.2018.00343.

D. Chen et al., "Gated context aggregation network for image dehazing and deraining," Proc. - 2019 IEEE Winter Conf. Appl. Comput. Vision, WACV 2019, vol. 00151, no. 1, pp. 1375–1383, 2019, doi: 10.1109/WACV.2019.00151.

Z. Liu, B. Xiao, M. Alrabeiah, K. Wang, and J. Chen, "Single Image Dehazing with a Generic Model-Agnostic Convolutional Neural Network," *IEEE Signal Process. Lett.*, vol. 26, no. 6, pp. 833–837, 2019, doi: 10.1109/LSP.2019.2910403.

X. Liu, Y. Ma, Z. Shi, and J. Chen, "GridDehazeNet: Attention-based multi-scale network for image dehazing," *Proc. IEEE Int. Conf. Comput. Vis.*, vol. 2019-Octob, pp. 7313–7322, 2019, doi: 10.1109/ICCV.2019.00741.

X. Qin, Z. Wang, Y. Bai, X. Xie, and H. Jia, "FFA-Net: Feature fusion attention network for single image dehazing," *AAAI 2020 - 34th AAAI Conf. Artif. Intell.*, pp. 11908–11915, 2020, doi: 10.1609/aaai.v34i07.6865.

S. Memon, R. H. Arain, and G. A. Mallah, "AMSFF-Net: Attention-Based Multi-Stream Feature Fusion Network for Single Image Dehazing," J. Vis. Commun. Image Represent., vol. 90, no. August 2022, p. 103748, 2023, doi: 10.1016/j.jvcir.2022.103748.

F. Chollet, "Xception: Deep learning with depthwise separable convolutions," *Proc. - 30th IEEE Conf. Comput. Vis. Pattern Recognition, CVPR 2017*, vol. 2017-January, pp. 1800–1807, 2017, doi: 10.1109/CVPR.2017.195.

P. Bassanini and A. R. Elcrat, "Elliptic Partial Differential Equations of Second Order," *Theory Appl. Partial Differ. Equations*, pp. 213–267, 1997, doi: 10.1007/978-1-4899-1875-8_5.

D. P. Kingma and J. L. Ba, "Adam: A method for stochastic optimization," *3rd Int. Conf. Learn. Represent. ICLR 2015 - Conf. Track Proc.*, 2015.

B. Li *et al.*, "Benchmarking Single-Image Dehazing and beyond," *IEEE Trans. Image Process.*, vol. 28, no. 1, pp. 492–505, 2019, doi: 10.1109/TIP.2018.2867951.

D. Scharstein and R. Szeliski, "High-accuracy stereo depth maps using structured light," *Proc. IEEE Comput. Soc. Conf. Comput. Vis. Pattern Recognit.*, vol. 1, 2003, doi: 10.1109/cvpr.2003.1211354.

N. Silberman, D. Hoiem, P. Kohli, and R. Fergus, "Indoor segmentation and support inference from RGBD images," *Lect. Notes Comput. Sci. (including Subser. Lect. Notes Artif. Intell. Lect. Notes Bioinformatics)*, vol. 7576 LNCS, no. PART 5, pp. 746–760, 2012, doi: 10.1007/978-3-642-33715-4_54.

F. Liu, C. Shen, G. Lin, and I. Reid, "Learning Depth from Single Monocular Images Using Deep Convolutional Neural Fields," *IEEE Trans. Pattern Anal. Mach. Intell.*, vol. 38, no. 10, pp. 2024–2039, 2016, doi: 10.1109/TPAMI.2015.2505283.

2026 by the authors; The Asian Academy of Business and social science research Ltd Pakistan. This is an open access article distributed under the terms and conditions of the Creative Commons Attribution (CC-BY) license (http://creativecommons.org/licenses/by/4.0/).